Energy Confinement Scaling in the Low Aspect Ratio National Spherical Torus Experiment (NSTX)

S.M. Kaye[1], M.G. Bell[1], R.E. Bell[1], E.D. Fredrickson[1], B.P. LeBlanc[1], K.C. Lee[2], S. Lynch[3], S.A. Sabbagh[4]

e-mail contact of main author: skaye@pppl.gov

Abstract

Systematic and statistical studies have been conducted in order to develop an understanding of the parametric dependences of both the global and thermal energy confinement times at low aspect ratio in high power NSTX discharges. The global and thermal confinement times of both L- and H-mode discharges can exceed values given by H-mode scalings developed for conventional aspect ratio. Results of *systematic scans* in the H-mode indicate that the confinement times exhibit a nearly linear dependence on plasma current and a power degradation weaker than that observed at conventional aspect ratio. In addition, the dependence on the toroidal magnetic field is stronger than that seen in conventional aspect ratio tokamaks. This latter trend is also evident in *statistical analyses* of the available dataset. These statistical studies also indicate a weaker parametric dependence on plasma current than found in the systematic scans, due to correlations among the predictor variables. Regressions based on engineering variables, when transformed to dimensionless physics variables, indicate that the dependence of $B\tau_E$ on β_T can range from being negative to null. Regressions based directly on the dimensionless physics variables are inexact because of large correlations among these variables. Scatter in the confinement data, at otherwise fixed operating parameters, is found to be due to variations in ELM activity, low frequency density fluctuations and plasma shaping.

[1]Princeton Plasma Physics Laboratory, Princeton University, Princeton, NJ 08543, USA
[2]University of California, Davis, CA, USA
[3]Dept. of Sociology, Princeton University, Princeton, NJ 08543, USA
[4]Dept. of Applied Physics, Columbia University, NYC, NY, USA

I. Introduction

The goals of the National Spherical Torus Experiment (NSTX)[1–4] are both to develop the physics basis for advancing the Spherical Tokamak (ST) concept, and to advance the understanding of toroidal confinement physics. The latter is to be accomplished, in part, by connecting results from NSTX to those from other magnetic confinement devices in order to understand confinement physics issues common to both configurations. To address these goals, NSTX operates at low aspect ratio (R/a) and routinely at high toroidal β_T ($=< p > /(B^2/2\mu_0)$, where $< p >$ is the volume-averaged pressure, and B can be defined as either the vacuum magnetic field at the geometric axis or the total magnetic field, $B_{TOT} = \sqrt{B_T^2 + B_{pol}^2}$). The ability to extend the conventional aspect ratio database in both β_T and R/a will help reduce the uncertainties in the inferred dependence of confinement with these parameters, and, consequently, may help reduce the uncertainty in confinement projections to future, larger devices such as ITER. Furthermore, operation in the coupled low aspect ratio, low field, high power regime will elucidate physics issues specific to enhanced toroidicity, kinetic effects and high β_T.

Confinement analysis of MAST data has recently been reported.[5] While MAST operation so far has been limited to lower beam power than that of NSTX, their main results indicate that their thermal energy confinement times generally agree with the ITER98P(y,2) scaling,[6] supporting the aspect ratio dependence implicit in that scaling ($(R/a)^{-0.58}$). The MAST confinement times show a favorable trend with decreasing collisionality. In this paper, the confinement trends of NSTX L- and H-mode discharges will be studied in the context of both engineering and physics variables, with the focus on H-mode discharges. Attempts will be made to identify the sources of scatter in the data at otherwise fixed operating conditions. The sources apparently responsible for the scatter include differences in ELM activity and low-frequency density fluctuations and in details of the plasma shaping. The NSTX data has been contributed to the international H-mode confinement database, and it has been used, in conjunction with MAST and START data, to determine the aspect ratio scaling of the thermal confinement time to a higher degree of certainty.[7] In this referenced work, the aspect ratio scaling derived from the database with low aspect ratio data included is stronger, and it is more favorable for low aspect ratio than the dependence on this parameter in, for instance, the ITER98P(y,2) scaling.

II. Experiment and Analysis Description

NSTX operates at low aspect ratio with nominal major radius R=0.85 m and minor radiuis a=0.67 m (R/a$\simeq$1.27). The data used for this study were taken from discharges run in the 2004 experimental campaign; the parameter ranges for this data are plasma current I_p=0.6 to 1.2 MA, toroidal magnetic field B_T=0.3 to 0.45 T, line-averaged density $\overline{n_e}$=1.5 to 7 $\times 10^{19}$ m^{-3} and elongation κ=1.7 to 2.4. The plasmas were heated by deuterium neutral beam injection (NBI) with powers from 1.5 to 7 MW (1 to 3 beam sources) at beam energies up to 100 keV. Because of the high beam injection energies, most of the absorbed neutral beam power ($\sim$2/3) heats the electrons directly, while only $\sim$1/3 heats the ions. Beam losses from shine-through, charge-exchange and birth onto orbits intersecting limiters ranged from 3.5 to 16% of the injected power for the highest to lowest currents in this dataset. Plasma operation for this study was in deuterium, and was in both the Lower Single Null (LSN) and Double Null (DN) divertor configurations for H-mode operation. In the LSN configuration, the ion ∇B drift was towards the X-point, leading to the lowest L-H threshold. L-mode plasmas were produced by limiting the plasma on the center stack. While up to 6 MW of High Harmonic Fast Wave power was available, only data from NBI discharges were used for this study. The β_T values (defined with respect to the vacuum toroidal field at the geometric axis) reached over 35% in the dataset, corresponding to values of the Troyon normalized β, β_N=β_T aB_T/I_p, of up to 6.8 %$\cdot$ m$\cdot$T/MA.

The global confinement times used in this study were derived from EFIT equilibrium reconstructions that were based on magnetic flux loop and sensor data.[8] The analyzed data (i.e., EFIT output) were backward time-averaged over 15 msec. The global confinement times were calculated from the backward time-averaged data (e.g., total stored energy and heating power). Thermal confinement times were calculated by TRANSP[9] using electron temperature and density profiles measured by the 20-point Thomson scattering system, and the ion temperature, density and rotation velocity profiles measured from CVI carbon emission by the 51-channel Charge-Exchange Recombination Spectroscopy (CHERS) diagnostic. Measurements from impurity survey instruments confirm that carbon is the dominant impurity in NSTX. The Z_{eff} profile was determined directly from the carbon density profile measured by CHERS. The beam heating profiles and fast ion energy content and losses were determined by a Monte-Carlo calculation with finite Larmor radius effects in TRANSP[10] assuming only classical collisional processes (i.e., no anomalous losses due to MHD activity). To test the validity of treating the fast ions classically, comparisons between the measured neutron fluxes and those calculated in the TRANSP model were made, since the neutron flux is predicted to be predominantly due to beam-target reactions. Agreement between

the measured and calculated neutron fluxes is within 10% for the data used in this study, supporting the assumption of classical processes only.

The thermal confinement times are defined as $\tau_{E,th}$=$W_{th}/(P_L - P_{f,loss})$, where W_{th} is the ion plus electron thermal stored energy, $P_L = P_{NBI} + P_{OH} - \dot{W}$, where P_{NBI} is the injected neutral beam power, $P_{f,loss}$ is the fast ion power lost due to shine-through, charge-exchange and bad orbit losses, P_{OH} is the ohmic heating power, and $\dot{W}$ is the time rate of change of the total stored energy. In the definition of P_L, the radiated power is not subtracted out, in keeping with historical convention. This is justifiable for NSTX, since the radiated power is low, typically only 5 to 15% of the total heating power. Furthermore, approximately half the radiated power comes from the outer 7 to 10 cm of the plasma, meaning that the radiated power fraction in the core, or "confinement region", is even smaller. The global confinement time is defined as τ_E=W_{tot}/P_L, where W_{tot} is the total stored energy as determined by the EFIT reconstruction. This W_{tot} implicitly includes the fast ion stored energy. These definitions are the same as those used in the International Confinement Database.[11] The average random uncertainties for the set of variables used in this study, (R, a, B_T, I_p, T_e, n_e, P_L, $P_{f,loss}$, τ_E, $\tau_{E,th}$) are approximately (2%, 3%, 1%, 2%, 6%, 5%, 10%, 15%, 15%, 20%). These uncertainties will be used later in the statistical analyses.

In LSN plasmas, only one source (1.5 to 2 MW) was typically needed to cause an L- to H-mode transition.[12] The H-mode phases, which exhibited low l_i and long durations of $q_0 > 1$, could last for up to 0.8 s, reaching a "steady-state" in terms of the stored energy evolution in discharges with small ELMs, but with densities slowly, but continuously, increasing to, typically, 80 to 90% of the Greenwald limit. Type I ELMs were seen at high power (low collisionality) and predominantly in DN discharges.[13,14] Typically, little or no difference in confinement time between LSN and DN plasmas was observed at similar operating conditions, although there was about a 10 to 20% reduction in confinement for ELMy (Type I and smaller ELMs) versus ELM-free discharges. L-mode discharges tended to have higher l_i and lower q_0, exhibiting low-frequency MHD activity after only 0.3 to 0.5 s of discharge duration at 0.45 T. At lower fields, the MHD activity set in even earlier. Consequently, these discharges tended to be more transient in terms of pulse length and $\dot{W}$ than the H-mode discharges.

III. Results

A. Single Parameter Scans

Examples of two 800 kA H-mode discharges used in this study are shown in Fig. 1. In the left panel are the time histories of representative parameters from a 0.45 T discharge, while

on the right are those from a discharge at 0.3 T. Plotted from top to bottom in each discharge are the time traces for the plasma current, neutral beam injection power, D_α emission, total stored energy, Greenwald density parameter (dashed line), line-averaged density (solid line) and the global confinement time normalized to the value given by the ITER97L scaling.[15] In the 0.45 T discharge, the heating power was 4 MW, and the L to H-transition occurred near 0.2 s. After a short ELM-free period, small ELMs developed at 0.28 s, and this period lasted for 0.14 s. At that time, larger Type I ELMs developed. During the small ELM period, the stored energy plateaued at 190 kJ, but the line-averaged density continued to increase, ultimately reaching 80% of the Greenwald limit. The global confinement time enhancement over the value given by the L-mode scaling, H_L, reached 2.2 in the beginning portion of the H-phase, and then decreased to $\sim$1.8 at the end of the small ELM phase. This particular discharge had a current flattop of 0.5 s, although, as mentioned, other H-mode discharges at this toroidal field had current flattops for up to 0.8 s.

The 0.3 T discharge was of much shorter duration, owing to an n=1 locked mode which developed at 0.3 s. This discharge had an L-to-H transition near 0.1 s with only 1.2 MW of injected power, and little ELM activity was seen until just after the third beam source was injected. During the ELM-free phase, both the stored energy and density increased, neither reaching a steady-state. The confinement enhancement factor was lower than that in the 0.45 T discharge, with H_L $\sim$1.5 throughout this phase. In this transient discharge, the $\dot{W}$ was approximately 0.6 MW, or 15% of the injected power, while in the 0.45 T case, $\dot{W} \approx 0$. Because the H-mode discharges at higher toroidal field were the least transient, and thus reflected more a steady-state confinement situation, systematic scans were performed in these plasmas to isolate the parametric dependences of both the global and local confinement times.

Systematic scans in the LSN configuration were performed holding toroidal field fixed and varying either the plasma current or heating power while holding the other fixed. To establish the scaling with plasma current, the neutral beam injection power was held constant at two different levels, approximately 4 MW (2 beam sources) and approximately 6 MW (3 beam sources). The magnetic field was fixed at 0.45 T and the plasma elongation at 2.1. Fig. 2 shows the results of the scan at 4 MW. The plasma current was scanned in four steps from 0.6 to 1.2 MA. In this set of discharges, the total stored energy, as determined by EFIT, and the electron stored energy as determined from Thomson scattering measurements, were both seen to increase with increasing plasma current; at 0.5 s, their values scale nearly linearly with plasma current. There was a brief drop-out in the injected beam power for the 1 MA discharge, although this did not affect the ultimate stored energy. The same linear dependence of total and electron stored energy with plasma current was observed

with injection powers of ∼6 MW. The density and temperature profiles taken near the time of peak electron stored energy (as denoted by the points on the respective time traces) are shown in the right-hand panels of the figure. The electron density varied by approximately 30% at these times over the range of currents, but the electron temperatures remained nearly constant except at the highest current. The "ears" on the density profile are caused by the buildup of carbon at the edge during the early and mid H-mode phases. The ears tended to dissipate as the central density increased during the latter phase of the H-phase and during periods of strong ELM activity. Carbon density buildup at the edge was observed to a lesser extent at conventional aspect ratio during DIII-D VH-modes.[16]

The energy confinement times from the systematic current scans at fixed power near 4 MW and magnetic field of 0.45 T, along with data from discharges with similar operating parameters, are plotted as a function of current in Fig. 3 for the H-mode plasmas. The results for both the global (left panel) and thermal (right panel) confinement times are shown. It is quite clear that both τ_E and $\tau_{E,th}$ scale nearly linearly with plasma current for this selection of data, ignoring any effects from the variation in density over this range of current. Similar plots of data at a fixed plasma current of 0.8 MA, but with varying heating power are shown in Fig. 4. The global confinement was found to degrade as $P^{-0.40}$, a degradation weaker than that determined statistically at higher aspect ratio.[6] However, the thermal confinement is seen to scale as $P^{-0.57}$, a slightly stronger degradation than for the global confinement time. While not enough L-mode data was obtained to perform single parameter studies as was done for the H-modes, a statistical analysis of the L-mode data indicates that the L-mode global confinement times also exhibited a nearly linear dependence on plasma current and a degradation with power going as $P^{-0.37}$. These statistical results will be discussed in the next section.

While the nearly linear dependence on plasma current and degradation with power is similar to the trends observed at conventional aspect ratio, contrary to conventional aspect ratio, however, a B_T dependence was seen in the NSTX dataset. This trend in the global and thermal confinement times is shown in Fig. 5, where the normalized confinement times for both L- and H-mode are plotted as a function of toroidal magnetic field at the geometric axis. The left panel shows the global τ_E normalized to the 97 L-mode scaling and the right panel shows the thermal τ_E normalized to the H-mode ITERH98P(y,2) thermal τ_E scaling. The figure shows that the global τ_E values are enhanced over the L-mode value, with enhancement factors of close to 2.8 at the highest toroidal field for both L- and H-mode plasmas. Although the confinement enhancements for L- and H-mode discharges are comparable, the L-mode discharges tended to have lower stored energies; their confinement times were comparable to those of similar parameter H-modes owing to the larger $\dot{W}$ and thus lower P_L for similar

absorbed+ohmic heating power.

The thermal confinement enhancement factors are more modest, reaching 1.4 at the highest B_T for H-mode plasmas, but with lower values at lower fields. The thermal τ_E values ranged from a factor of 0.36 to 1.13 of the global τ_E, with a mean value of 0.66. Only a few discharges have $\tau_{E,th} > \tau_{E,global}$, and these are at low power and low density where the fractional fast ion loss power is greater than the fractional fast ion stored energy. The quality of the kinetic data for L-modes at the lowest B_T precluded calculating the thermal τ_E at these fields for these discharges with confidence. A reduction in confinement enhancement at low B_T is evident in the H-mode plasmas for both the global and thermal values; this reduction in confinement enhancement at lower toroidal magnetic field was also seen in datasets from prior year's experiments. We note that lower B_T is associated with higher values of various dimensionless parameters such as ρ_*, ν_* and β_T. However, there was no discernable dependence of the confinement on proximity to the beta limit, β_N, for the range of toroidal fields studied. The functional dependence of the confinement on these parameters will be discussed in the next section.

The general increase in the enhancement factor with increasing B_T is associated with a reduction in the ratio of the electron to ion thermal diffusivities, χ_e/χ_i, at r/a=0.4. This ratio decreased from an average value of 10 to 15 at B_T=0.3 T to an average value of 4 to 5 at B_T=0.45 T. These average ratios reflect the dominance of electron transport at all toroidal fields.

It is seen in Fig. 5 that there is considerable scatter in the confinement enhancement factors, even at fixed toroidal field. For instance, enhancements are seen to vary by a factor of two at 0.45 T. Five possible sources for the data scatter in H-mode discharges were considered: plasma rotation, magnetic fluctuations, ELMs, plasma shape and density fluctuations. This study focused on H-mode data since this dataset was more complete than that for L-modes. The thermal confinement enhancement factor for the H-mode discharges, H_H, was found to increase with increasing central rotation velocity when data from all toroidal fields was included. However, the central rotation velocity itself was observed to be a strong function of B_T. The reason for this is that as the toroidal field increases, the pulse duration also increases, giving the plasma time to spin up to higher velocities. At the fixed toroidal field of 0.45 T, however, there is no ordering of the data or reduction in the data scatter by the rotation velocity.

The effect of magnetic fluctuations on the plasma confinement was studied using the signal from a Mirnov coil located on the outer vessel wall 45 cm above the midplane with the data sampled at 10 MHz. For this study, signal amplitudes ($\dot{B}$) in three frequency ranges were calculated: 5 to 50 kHz to reflect low frequency MHD activity including tearing and

kink modes, 80 to 120 kHz spanning the toroidal Alfvén eigenmode range of frequencies, and 300 kHz to 2 MHz to capture Compressional and Global Alfvén eigenmodes. Similar to the results for the toroidal rotation velocity, there was no apparent dependence of H_H at fixed toroidal field on the magnetic activity at the times of interest in any of the three frequency ranges.

As in devices at conventional aspect ratio, the severity and type of ELM activity could impact the confinement enhancement. The H-mode discharges in NSTX could either be ELM-free, or they could contain Type I or smaller ELMs. Type I ELMs generally occurred in DN plasma or plasmas with high NBI power at low collisionality. At higher collisionality, the ELMs tended to be Type III or Type V.[13,14] The H_H factors are plotted as a function of ELM spectral power for discharges at 0.45 T in Fig. 6 (left panel). Here, the ELM spectral power represents the frequency-space integrated fluctuation amplitude of the D_α signal during the ELM. Zero ELM amplitude means that the H-mode was ELM-free. It has been shown previously that for NSTX, the average energy lost during the ELMy period is proportional to the ELM amplitude as based on the D_α signal.[13,14] While there is clearly no simple linear relation between H_H and ELM amplitude, the confinement enhancements do depend on ELM type and amplitude in an average sense. For instance, the average H_H factor for ELM-free discharges is 1.1, although the scatter still remains a factor of two. The ELMy discharges have lower average H_H factors, being 0.9 for discharges with small ELMs and approximately 0.75 for discharges with giant (Type I) ELMs. The scatter in both these latter groups of points is less than that for the ELM-free discharges. The H_H factor has also been studied as a function of simply the ELM frequency, f_{ELM}, as has been done in MAST.[17] For NSTX, the H_H factor remained relatively constant for f_{ELM} >100 Hz, while H_H was degraded for f_{ELM} <100 Hz; the latter frequency range reflects the Type I ELM regime in NSTX. This contrasts with the results from MAST, which show a secular decrease in H_H with increasing ELM frequency in the Type III ELM regime.

The right hand panel of Fig. 6 shows the confinement enhancement also as a function of ELM amplitude, but sorted by plasma elongation κ. As can be seen, the confinement enhancement is also influenced by plasma shape in this dataset. While the range of elongation for this dataset was narrow, and therefore elongation was not included as a predictor variable in the statistical analyses, the figure on the right shows that the enhancement factor was lower for more highly elongated plasmas. This means that the confinement time itself scaled significantly weaker than the $\kappa^{0.78}$ in the IPPB98(y,2) scaling. This is most clearly seen for ELM-free discharges, as the dependence of ELM-type on κ complicates the interpretation for the subset of discharges which do have ELMS. A more precise determination of the κ-scaling in NSTX will be studied in future experiments.

Another potential source of scatter was studied by examining the relation between the confinement enhancement factor and density fluctuations in the plasma. Here, the comparison is made to the density fluctuation amplitude only; no measurements of the associated potential fluctuations or the correlation between the density and potential fluctuations were available. The density fluctuation spectra were computed from a far-infrared interferometer measurement along a chord with a tangency radius of R=0.85 m; the sightline of this chord accesses the core region of the plasma. The interferometer can detect fluctuations up to 200 kHz. Plotted in Fig. 7 (left panel) is the H_H factor as a function of average power (in arbitrary units) of the density fluctuation level averaged over 15 ms in the frequency range from 5 to 20 kHz for all three groups of H-mode points. The confinement enhancement is seen to depend on the fluctuation level. There is, however, some dependence of the density fluctuation amplitude on the ELM type. Although the lowest density fluctuation amplitudes were associated with ELM-free discharges, some of these discharges exhibited higher fluctuation amplitudes as well, and this latter set were well mixed with the ELMy discharges. All three types showed a general decrease of confinement enhancement factor with fluctuation amplitude. No dependence of H_H on fluctuation level at higher frequencies was found. Although the density measurement was from a line-integrated signal from the outside of the plasma, there was no interferometer chord that measured local fluctuation levels in the outer part of the plasma; the next most outer viewing chord had a tangency radius of 1.5 m, which was generally in the scrape-off layer for most of these plasmas. No dependence of H_H on density fluctuation level as measured by this SOL viewing chord was observed, indicating that the source location of the density fluctuations was within the closed flux region. The low frequency density fluctuations could reflect MHD activity internal to the plasma that was not well detected by magnetic pickup loops situated outside the plasma. When the density fluctuation amplitude is normalized by the line-averaged density, $\overline{n}_e$, as seen in the right-hand panel of Fig. 7, the correlation still exists, albeit weaker. Future experiments will take advantage of the measurements from a tangential scattering system, which will give a picture of turbulence from the upper end of the ITG/TEM regime ($k_\theta \rho_i \sim 2$) to high-k ETG modes ($k_\theta \rho_i$ up to 20).

B. Statistical Analysis

Statistical analysis of confinement data is usually done through Ordinary Least Squares Regression (OLSR) analysis in which a power law functional fit is assumed. The OLSR analysis assumes perfect knowledge of both the independent (predictor) variables and the dependent (response) variable (i.e., no uncertainties in their values). Other techniques, which

incorporate "errors-in-variables", can be employed, however. In one such technique,[18] the principal components of the logarithms of the full variable set (both predictor and response variables) are determined, with the logarithms of the variables weighted by their uncertainties, which are taken to be symmetric about the logarithm of the data and uncorrelated. A linear relation among the logarithms of the variables can be determined from the principal component, or eigenvector, that is associated with the minimum eigenvalue (if very small). This ability to form a linear relation among the variables allows a determination of the functional relation between the response variable and the set of predictor variables. Uncertainties in the scaling coefficients cannot be determined from a straightforward application of this method. Furthermore, the assumption that the the errors are symmetric about the logarithms of the data may introduce some bias in the fit. This Principal Component Error-In-Variable (PCEIV) technique has been used to analyze confinement data from the International Tokamak Confinement Database.[19,20,7] Finally, a Bayesian approach,[21] in which the uncertainties are built directly into the model, can be used. In the Bayesian approach, the actual data value is assumed to be contained within a normal distribution centered about each measurement value. The measurement error is related to the standard deviation of this distribution so that 99% of all possible values of the observation is contained within the measurement error. The Bayesian method gives an almost identical result to the OLSR method, and so results from only the OLSR and PCEIV methods will be presented here.

In the first set of analyses, engineering parameters (I_p, B_T, $\overline{n}_e$ and $P_{L,th}$) were used as predictor variables, and $\tau_{E,th}$ was used as the response variable. Among the predictor variables, a strong colinearity was observed only between $\overline{n}_e$ and $P_{L,th}$, with a correlation coefficient between the two variables of 0.74. This means that the exponents determined from these variables are interdependent, as will be demonstrated.

The NSTX dataset was subselected so that only discharges with beam energy fractions less than half of the total stored energy were analyzed, consistent with constraints put on the data from the international confinement database. The OLSR analysis of the 85 NSTX H-mode points (both ELMy and ELM-free) that satisfy this constraint yields a scaling relation

$$\tau_{E,th} \sim I_p^{0.57} B_T^{1.08} \overline{n}_e^{0.44} P_{L,th}^{-0.73} \tag{1}$$

with a RMSE=0.145. Here, the RMSE, or Root Mean Square Error, is defined as $\sum_{i=1}^{N} \sqrt{\frac{(y_{exp}-y_{fit})^2}{N-2}}$, where y_{exp} is the experimental value and y_{fit} is the value from the scaling.

Omitting $\overline{n}_e$ yields the relation

$$\tau_{E,th} \sim I_p^{0.70} B_T^{1.21} P_{L,th}^{-0.58} \tag{2}$$

with a goodness-of-fit almost as good as that with all four predictor variables included. Both expressions exhibit the strong toroidal field dependence evident in the dataset. The dependence on plasma current in these statistical analyses is less than linear. This contrasts with the linear dependence found in systematic scans (i.e., Fig. 3), and it can be the result of correlations between variables. In this case, the correlation coefficient between I_p and $\overline{n}_e$ over their full range is 0.53, which is enough to impact the statistically determined parametric dependences. The power dependence in both scalings is similar to that found in conventional aspect ratio tokamak scalings. Dropping the density as a predictor variable has a significant effect on the power dependence, reflecting the correlation also between these two variables.

Uncertainties in both the predictor and response variables have been taken into account in the OLSR approach by artificially expanding the dataset by a factor of five for each observation. This was done for each observation by randomly varying the variable values (predictor and response) within their uncertainties, and using the result as a "new" observation. Results of the OLSR on this expanded dataset, including $\overline{n}_e$ as an independent variable, gave a scaling very similar to that given in Eq. 1, but with a slightly lower RMSE.

Finally, for the engineering variables, the PCEIV approach was also used to determine the parametric scaling relation of the energy confinement. In this approach, W_{th}, not $\tau_{E,th}$, was used in addition to the other parameters to determine the scaling since W_{th} is more of a measured than computed quantity. The $\tau_{E,th}$ fit was determined from the linear dependence of $\ln W_{th}$ on the logarithms of the other variables. The results of this approach yield the relations

$$\tau_{E,th} \sim I_p^{0.52} B_T^{0.87} \overline{n}_e^{0.27} P_{L,th}^{-0.50} \tag{3}$$

with a RMSE=0.158, and without $\overline{n}_e$,

$$\tau_{E,th} \sim I_p^{0.56} B_T^{0.63} P_{L,th}^{-0.40} \tag{4}$$

As can be seen, the degradation with power is weaker than that from OLSR, and it is significantly weaker than that observed on conventional aspect ratio tokamaks. Despite the differences in the scaling expressions determined from the OLSR and PCEIV, the goodness-of-fits, as reflected by the RMSE values, are comparable, again suggesting that trade-offs among the scaling coefficients result from interdependences among the predictor variables. It is noted that restricting the dataset to only ELMy discharges leads to scalings, by either method, similar in parametric dependence and goodness-of-fit as for the full dataset (ELMy

and ELM-free). A summary of the fits using engineering parameters as the predictor variables is given in Table 1, and fits to the OLSR and PCEIV scalings are shown in Fig. 8.

The scalings based on engineering variables can be converted to relations that are described by dimensionless, or physics, variables. These variables are believed to be more closely related to the underlying physics controlling plasma transport, and may allow for higher confidence extrapolations to future devices. The set of physics variables chosen are: ρ_* ($\propto T^{1/2}/B$), $\beta_{th,TOT}$ ($\propto W_{th}/B^2$), ν_* ($\propto \overline{n}_e q/T^2$), and q for fixed geometry. In this transformation, the dataset is assumed to satisfy a Kadomtsev constraint[22] so that $\tau \sim \tau_{Bohm} f(\rho_*,\ \beta_T,\ \nu_*,\ q)$, where $\tau_{Bohm} \propto B/T$. The transformations of the scalings that contain the density as a predictor variable (Cases 1, 2 4 and 5) in Table 1 are given in Table 2. In this table, it is the normalized confinement $B\tau$ that is expressed in terms of the dimensionless variables. Of particular significance is the β-dependence, which, for the full dataset, is seen to vary from strongly unfavorable (Case 1 using the OLSR analysis method), to essentially null (Case 3 using the PCEIV analysis method). The β-dependence of confinment is an active subject of research for ITER that is still unresolved,[20,19,23,24,7] since the resulting dependence is sensitive to both the dataset selected and the method of analysis. Dedicated β scans are planned for a future NSTX experimental campaign.

While the set of engineering variables used as the predictor variables in the above scaling expressions are useful in that those are the parameters that are controllable in experiments, the dimensionless physics variables could be used as well. For this analysis, these parameters were calculated based on volume-averaged values of electron temperature and density, the total thermal stored energy, W_{th}, and the total magnetic field, B_{TOT}, which is approximated by $\sqrt{B_{pol}^2 + B_T^2}$, where B_{pol} is the poloidal field at the edge (computed from q) and B_T is the vacuum magnetic field at the geometric axis. It is important to include both components of the magnetic field for NSTX, as they can be comparable over the outer portion of the plasma. The cylindrical q-value, $q_{cyl} \sim (1+\kappa^2)a^2 B_T/RI_p$ was used explicitly and in the definition of ν_* for this statistical analysis of NSTX data. Here, the usual definition of κ (vertical/horizontal radius) was used in the definition of q_{cyl}.

The fits to the physics parameters reveal dependences that are different than those seen in Table 2, most notably in the β-dependence, which becomes a favorable one, with $B\tau \sim \beta_{th,TOT}^{0.6-1.0}$. However, it is important to note that, in general, the correlations between each individual dimensionless predictor variable and the other predictor variables are greater than that with the response variable, $B\tau$. This indicates a high degree of uncertainty in the resulting coefficients and fits. For instance, when using the dimensionless variables directly, there are large ranges of coefficients that can lead to good fits. Consequently, only fits based on the engineering variables will be presented.

The effect that the data uncertainties have on the fits can be explored by varying the uncertainties and redoing the fits. For this exercise, the PCEIV method, which gives a null dependence of $B\tau$ on β (Case 4, Table 2) was used, only the uncertainties on the variables with the largest relative errors (0.15 on W_{th} and 0.18 on $P_{L,th}$) were varied by $\pm 33\%$. The result of this showed that the largest variations in the engineering parameter scaling coefficients were in $\overline{n}_e$ and $P_{L,th}$. The I_p and B_T scaling coefficients varied by only a few percent. The $\overline{n}_e$ coefficient varied by ± 0.18, with a corresponding linear variation in the $P_{L,th}$ coefficient of ∓ 0.13. When transformed to physics variables, the largest variations are seen in the β and q coefficients, with the β coefficient varying by ± 0.13 with a corresponding linear variation in the q-coefficient by ∓ 0.40. The variation in the β coefficient gives a β dependence that ranges from slightly favorable to slightly unfavorable for this method.

An OLSR analysis of the NSTX L-mode data was performed as well, but using only the global confinement times since the data quality precluded a determination of the thermal stored energy, especially at low toroidal field. The results of this regression are shown graphically in Fig. 9, where the experimentally determined global confinement time is plotted as a function of the value obtained from the scaling expression

$$\tau_E \sim I_p^{1.01} B_T^{0.70} \overline{n}_e^{0.07} P_{loss}^{-0.37} \tag{5}$$

where, here $P_{loss} = P_{NBI} + P_{OH} - \dot{W} - P_{shine-thru}$. The fit has a RMSE=0.200. A significant toroidal field dependence emerges from the L-mode data also, although a linear dependence with plasma current nevertheless is seen in this statistical treatment. The power degradation of confinement here, too, is weaker than that at conventional aspect ratio.[15]

IV. Summary and Conclusions

Both systematic and statistical studies have been carried out in high power NSTX plasmas in order to develop an understanding of the confinement trends at low aspect ratio. The global and thermal confinement times can exceed values given by scalings developed from higher aspect ratio devices for both L- and H-modes, such as the ITER98P(y,2) scaling and scalings developed in Cordey et al..[20] The parametric scalings of these fits, however, are not entirely appropriate for the low aspect ratio regime. While systematic scans indicate dependences on plasma current and heating power that are similar to those at higher aspect ratio, statistical analyses indicate a weaker plasma current dependence, due in part to a correlation between plasma current and density. The most notable difference seen between the trends in the NSTX data and those at higher aspect ratio is a a significant dependence

on toroidal magnetic field. This dependence is related to a reduction in the core electron transport relative to that of the ions as B_T increases. These parametric dependences translate into favorable dependences with decreasing ρ_* and ν_* , and a β-dependence that varies from unfavorable to null, depending on the specific statistical analysis used. The dependences on the physics variables in NSTX are consistent with those dependences seen at higher aspect ratio.[19,20,7] Various sources of scatter in the NSTX data have been identified, and these include ELM severity, plasma shape and low frequency density fluctuations.

The NSTX data has been, and will continue to be, used in conjunction with higher aspect ratio data to determine the explicit dependence of confinement on aspect ratio and on β. A significant contribution made by NSTX is to extend the range of β of conventional aspect ratio devices by a factor of five, and this data, along with high neutral beam power data from MAST, is especially important in establishing the scaling with this parameter. As is seen in this work, the various statistical analyses still result in uncertainty about the precise β scaling, and this indicates the importance of performing systematic scans of this and other dimensionless parameters, and these are planned for a future NSTX experimental campaign. Also planned are experiments in which the density variation is decoupled from that of the current, as well as dedicated scans of the toroidal field, to establish the dependence of confinement on these parameters with greater confidence.

ACKNOWLEDGEMENTS

This work was supported by US Department of Energy Contract DE-AC02-76CH03073 at the Princeton Plasma Physics Laboratory, DE-FG02-99ER54518 at UC Davis and DE-FG02-99ER54524 at Columbia University. The authors would like to thank the entire NSTX operations, physics and engineering teams for their contributions to this effort.

References

[1]ONO, M., et al., Plasma Phys. Controlled Fusion **45**, A335 (2003).

[2]SYNAKOWSKI, E.J., et al., Nucl. Fusion **43**, 1653 (2003).

[3]ONO, M., et al., Nucl. Fusion **44**, 452 (2004).

[4]KAYE, S.M., et al., Nucl. Fusion **45**, S168 (2005).

[5]VALOVIC, M., et al., Nucl. Fusion **45**, 942 (2005).

[6]ITER Physics Basis, Nucl. Fusion **39**, 2137 (1999).

[7]KAYE, S.M. et al., Plasma Phys. Controlled Fusion **48**, A429 (2006).

[8]SABBAGH, S.A., et al., Nucl. Fusion **41**, 1601 (2001).

[9]HAWRYLUK, R.J., (Physics of Plasmas Close to Thermonuclear Conditions (Proc. Course Varenna, 1979), 1979, Vol. 1, p. 19.

[10]GOLDSTON, R.J., D.C. McCUNE, H.H. TOWNER, S.L. DAVIS, R.J. HAWRYLUK, et al., J. Comput. Phys. **43**, 61 (1981).

[11]CHRISTIANSEN, J.P., J.G. CORDEY, K. THOMSEN, A. TANGA and the JET Team, J.C. DEBOO, D.P. SCHISSEL, T.S. TAYLOR and the DIII-D Research Team, O.J.W.F. KARDAUN, F. WAGNER, F.RYTER and the ASDEX Team, S.M. KAYE and the PDX and PBX-M Teams, Y. MIURA, N. SUZUKI, M. MORI, T. MATSUDA, H. TAMAI, T. TAKIZUKA, S.-I. ITOH, K. ITOH and the JFT-2M Group, Nucl. Fusion **32**, 291 (1992).

[12]MAINGI, R., et al., Plasma Phys. and Controlled Fusion **46**, A305 (2004).

[13]MAINGI, R., et al., Nucl. Fusion **45**, 264 (2005).

[14]MAINGI, R., et al., Nucl. Fusion **45**, 1066 (2005).

[15]KAYE, S.M., et al., Nucl. Fusion **37**, 1303 (1997).

[16]WHYTE, D.G., et al., Nucl. Fusion **38**, 387 (1997).

[17]KIRK, A., et al., Plasma Phys. and Controlled Fusion **46**, 551 (2004).

[18]ANDERSON, T.W., Annals of Statistics **12**, 1 (1984).

[19]THOMSEN, K., J.G. CORDEY, O.J.W.F. KARDAUN and the ITPA H-Mode Database Working Group, Analysis of the bias in h-mode confinement scaling expressions related to measurement errors in variables, (Proc. 31st Eur. Physical Soc. Mtg. on Plasma Physics, London, 2004), 2004, Paper P3.145.

[20]CORDEY, J.G., et al., Nucl. Fusion **45**, 1078 (2005).

[21]GELMAN, A., J. CARLIN, H. STERN and D. RUBIN, Bayesian data analysis, 2nd Ed (Boca Raton: Chapman and Hall/CRC, 2004.

[22]CONNOR, J.W. and J.B. Taylor, Nucl. Fusion **17**, 1047 (1977).

[23]PETTY, C.C., T.C. LUCE, et al., Phys. Plasmas **11**, 2514 (2004).

[24]McDONALD, D.C., et al., Plasma Phys. and Controlled Fusion **46**, A215 (2004).

Case	Method	Coef	α_{I_p}	α_{B_T}	α_{n_e}	$\alpha_{P_{L,th}}$	$RMSE$
1	OLSR	4.69e-9	0.57	1.08	0.44	-0.73	0.145
2	OLSR (ELMy)	3.77e-9	0.58	1.01	0.43	-0.70	0.133
3	OLSR	4.24e-2	0.70	1.21	-	-0.58	0.150
4	PCEIV	5.11e-7	0.52	0.87	0.27	-0.50	0.158
5	PCEIV (ELMy)	1.59e-10	0.58	0.87	0.48	-0.68	0.136
6	PCEIV	1.44e-2	0.56	0.94	-	-0.40	0.163

Table 1: Scaling results for thermal energy confinement time with engineering parameters as the set of predictor variables. The units for I_p, B_T, $\overline{n}_e$, $P_{L,th}$ and $\tau_{E,th}$ are A, T, m^{-3}, W and sec respectively. In cases 3 and 6, the density has been ignored as a predictor variable

Case	Method	α_{ρ_*}	$\alpha_{\beta_{th,t}}$	α_{ν_*}	α_q
1	OLSR	-5.81	-0.65	-0.43	-1.69
2	OLSR (ELMy)	-5.31	-0.49	-0.41	-1.53
4	PCEIV	-3.75	-0.02	-0.45	-0.60
5	PCEIV (ELMy)	-4.92	-0.30	-0.32	-1.49

Table 2: Transformation of scaling coefficients from Table 1 from engineering to dimensionless physics variables.

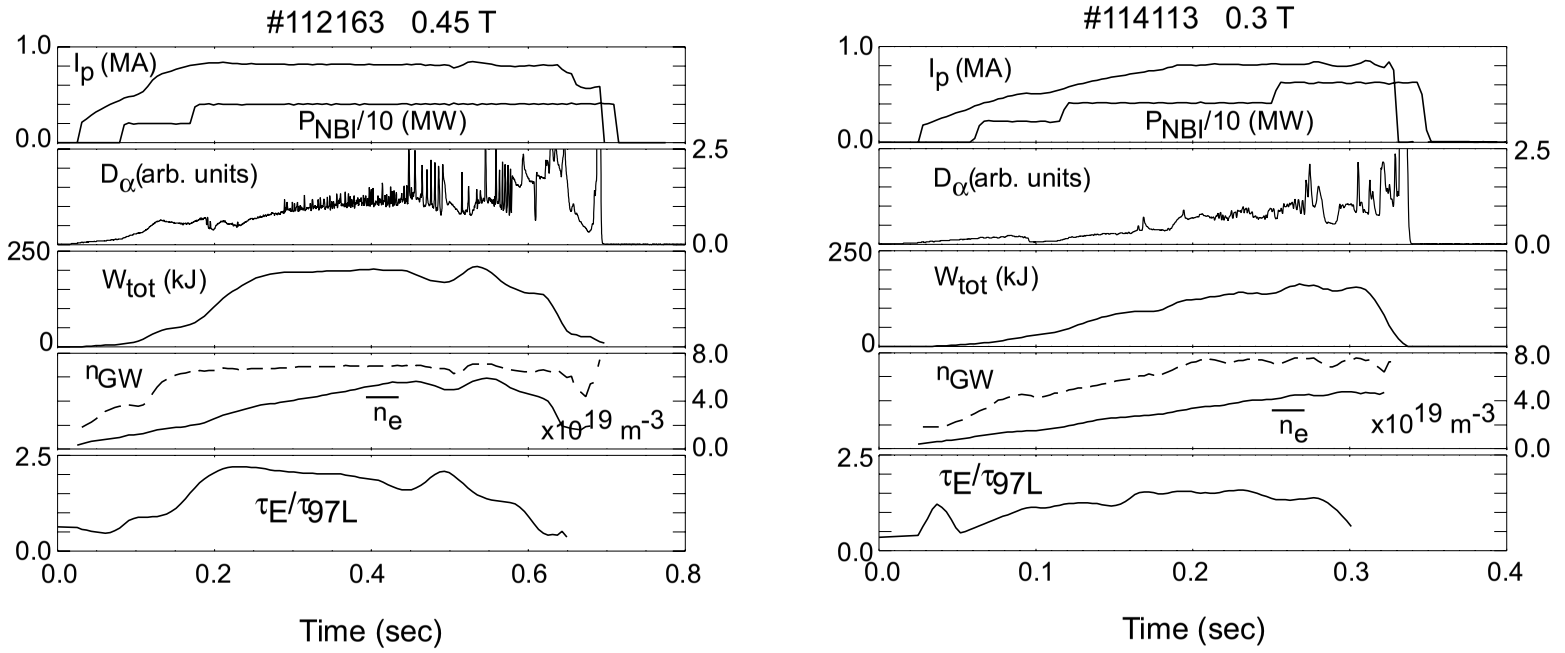

Figure 1: Evolution to H-mode discharges at 0.45 T (left panel) and 0.3 T (right panel). Plotted are the plasma current, neutral beam heating power, D_α emission, Greenwald density (dashed line), line-averaged density (solid line), and the global confinement time normalized to the value given by the ITER97L scaling expression for both discharges.

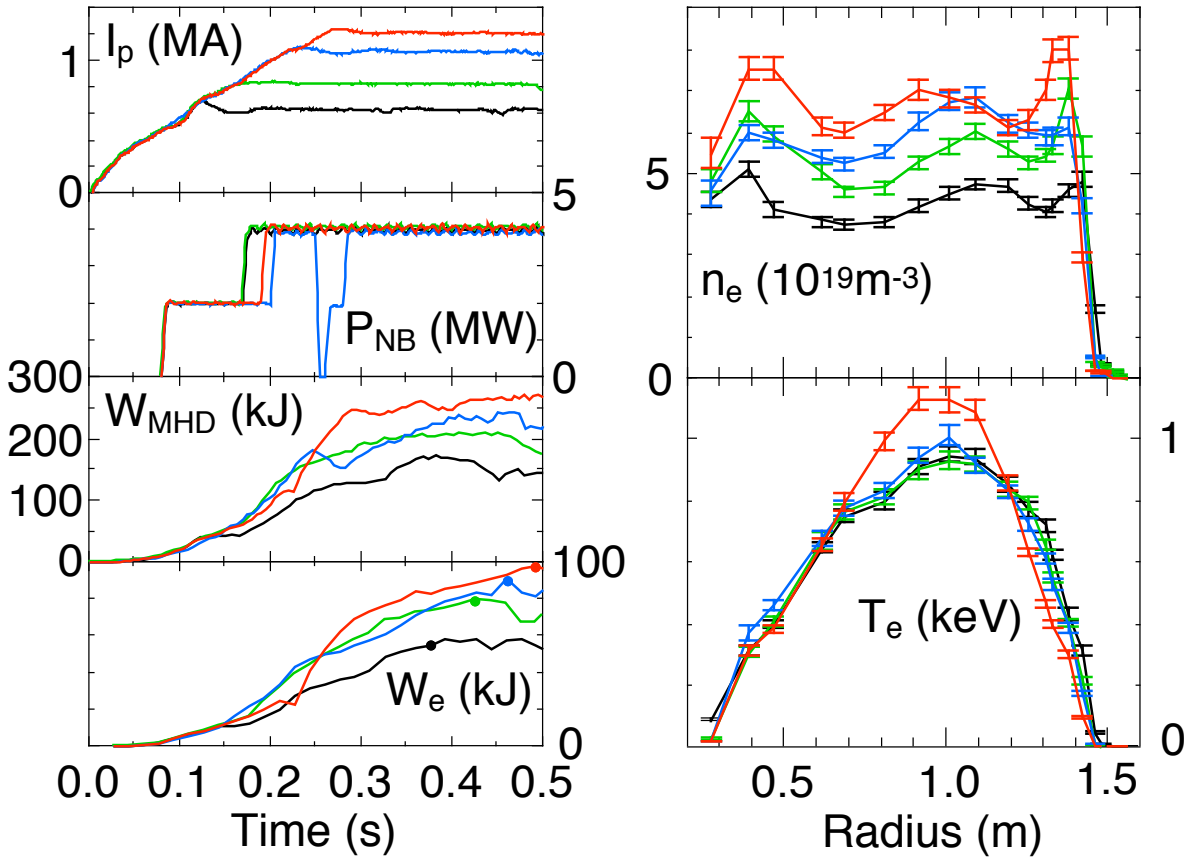

Figure 2: Plasma and electron stored energy evolutions for discharges from a systematic current scaling experiment at fixed neutral beam power. Also shown are the electron temperature and density profiles for these discharges near the time of peak electron stored energy.

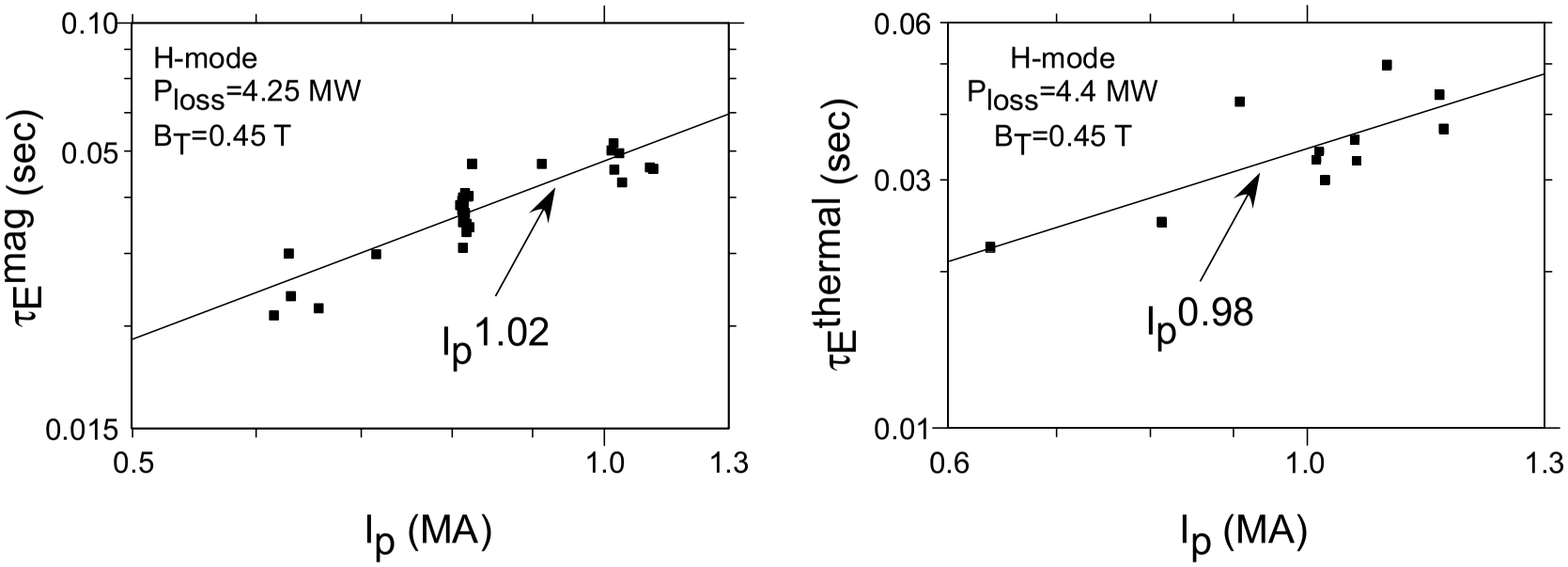

Figure 3: Dependence of global (left panel) and thermal (right panel) energy confinement times on I_p at fixed B_T and input power.

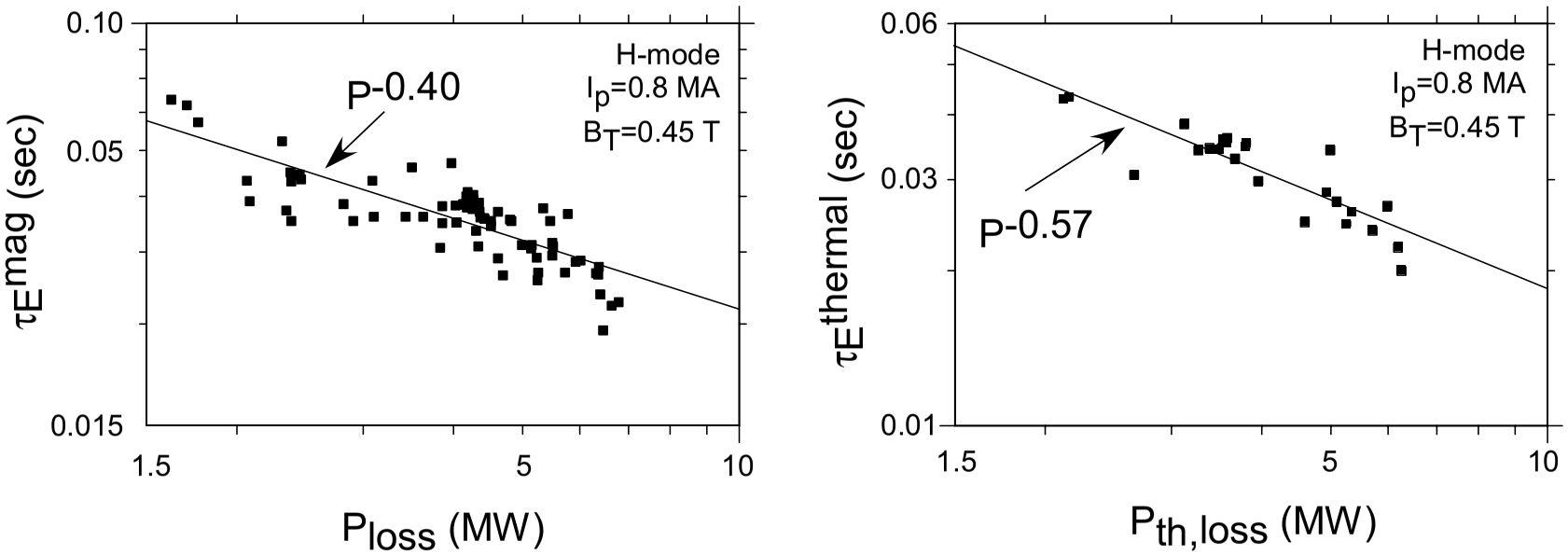

Figure 4: Dependence of global (left panel) and thermal (right panel) energy confinement times on heating power at fixed B_T and I_p. P_{loss} is the total input heating power less dW/dt and shine-thru, while $P_{th,loss}$ is the total input heating power less dW/dt and fast ion losses through charge-exchange, bad orbits and shine-through.

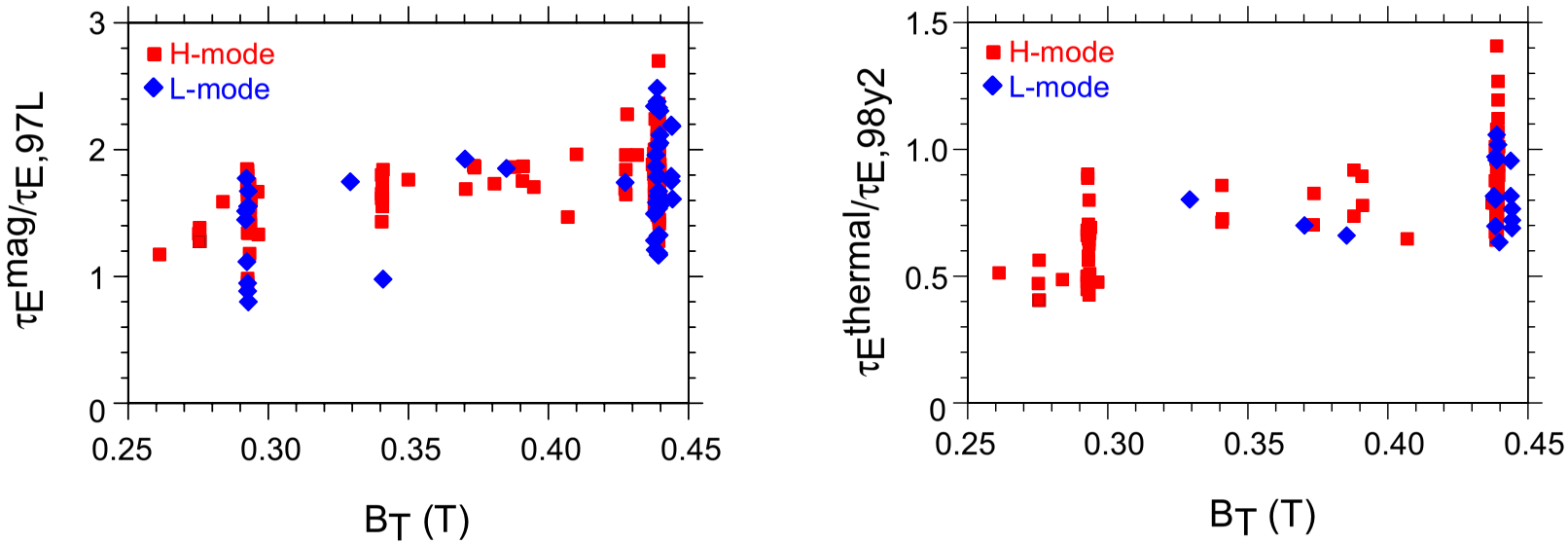

Figure 5: Global energy confinement time normalized to the 97L L-mode scaling value (left panel) and thermal confinement time normalized to the 98P(y,2) scaling (right panel) plotted as a function of toroidal field.

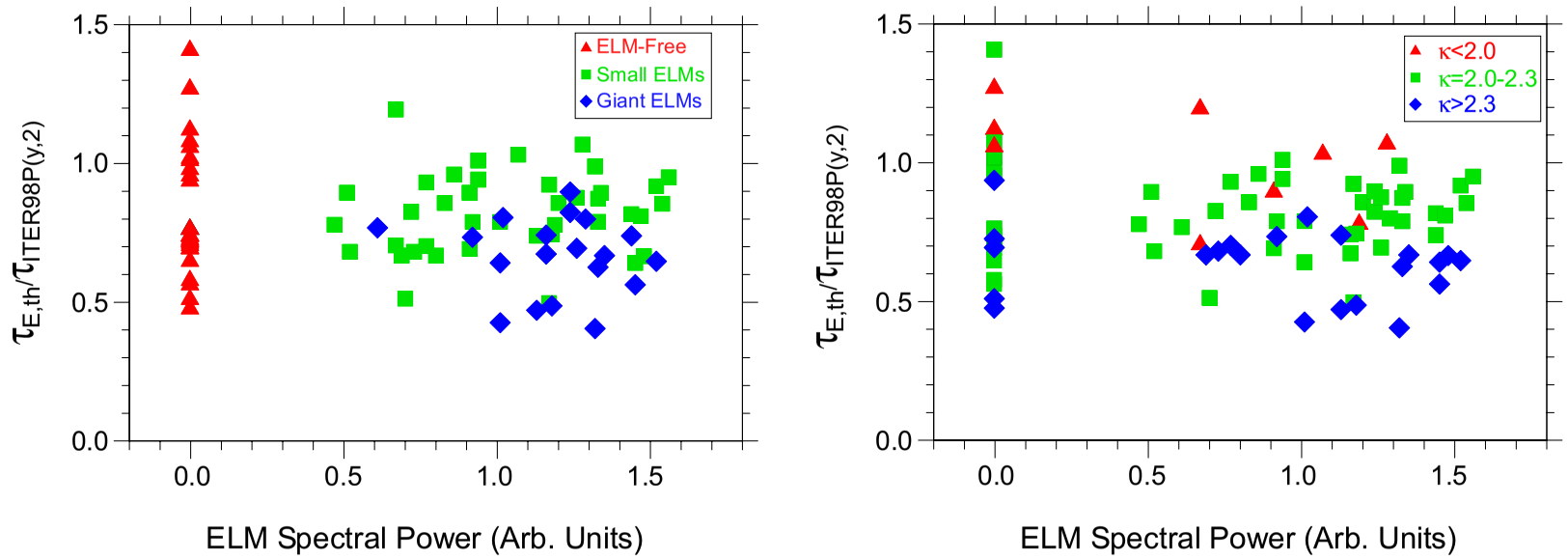

Figure 6: Thermal energy confinement time normalized to the value given by the ITER98P(y,2) scaling plotted versus ELM amplitude, sorted by ELM type (left panel) and plasma elongation (right panel).

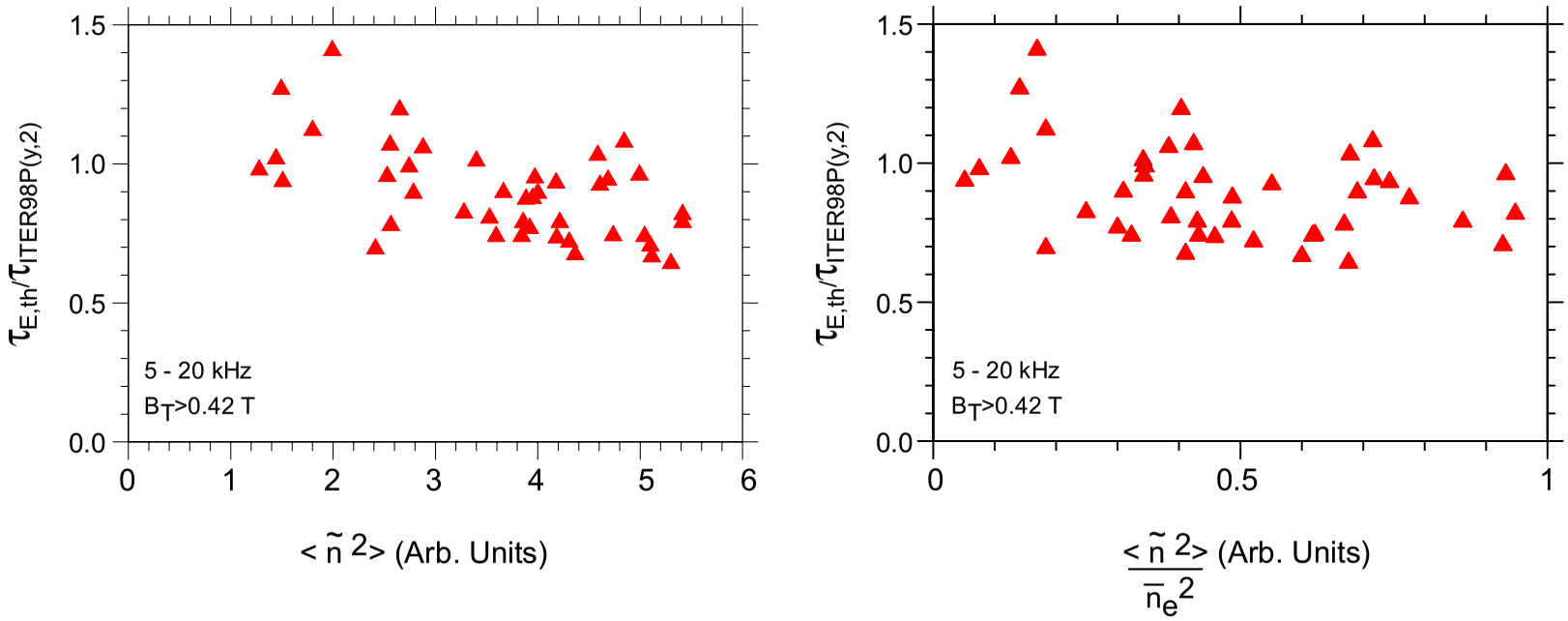

Figure 7: Thermal energy confinement time normalized to the value given by the ITER98P(y,2) scaling plotted versus density fluctuation amplitude (left panel), as measured by far-infrared interferometry, and the density fluctuation amplitude normalized to the line-averaged density (right panel) in the 5 to 20 kHz frequency range and for B_T=0.45 T.

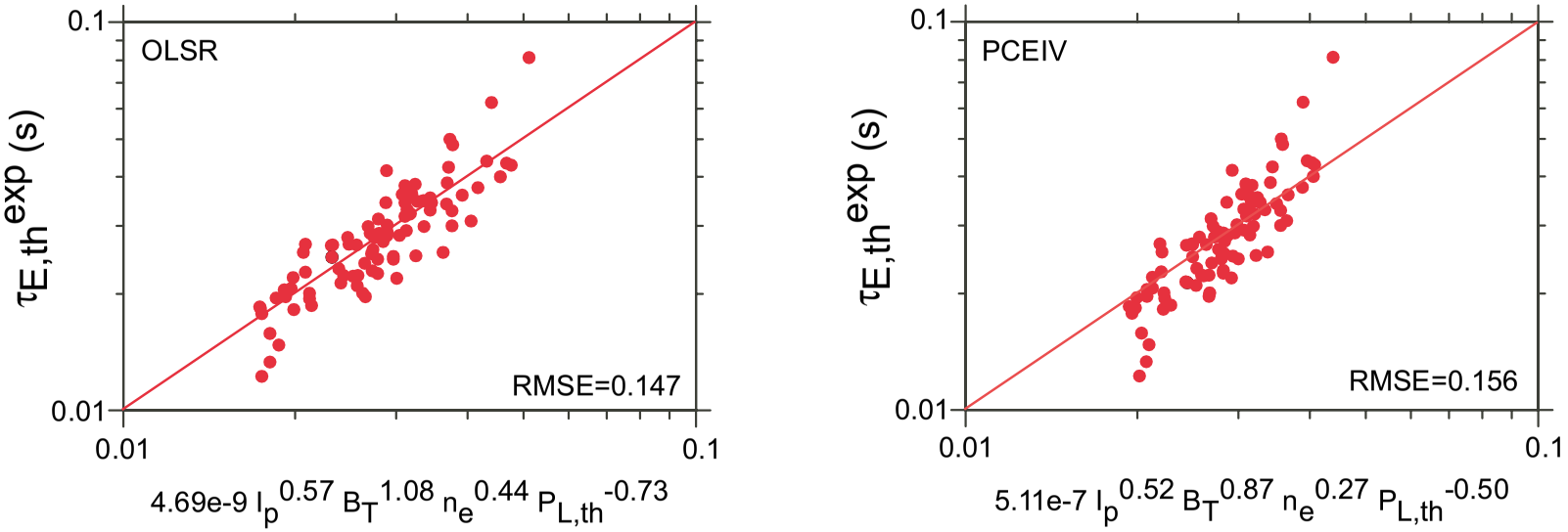

Figure 8: Thermal energy confinement time plotted as a function of value derived from scaling fits for the OLSR (Case 1, left panel) and PCEIV (Case 4, right panel) methods.

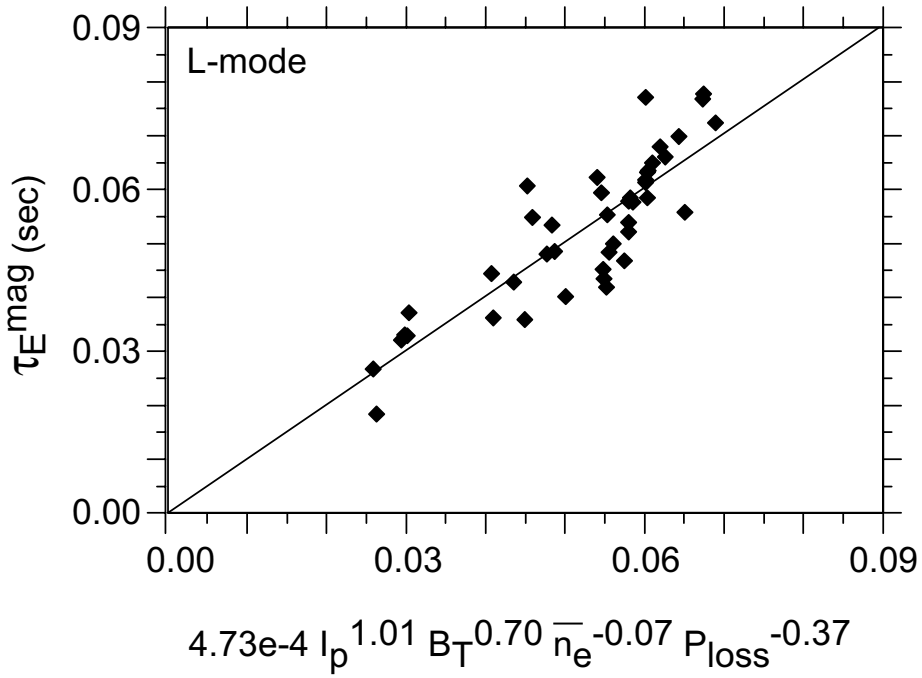

Figure 9: Experimental τ_E plotted versus the value given by the OLSR scaling for L-modes.